Chapter 4

NSST domain feature descriptors that uses bit-plane decomposition for biomedical image retrieval

With advancement in technology, biomedical images such as X-ray, CT scan, MRI, ultrasound images are able to capture visual representation of interior human body parts effectively and these images play crucial role in diagnosis of different diseases. Appropriate exploitation of these images necessitates the accurate feature representation for efficient retrieval strategies. Biomedical images consists of complicated structural and spatial details and to extract these significant details, different approaches have been introduced in the literature both in spatial and transform domain. Since NSST offers nearly optimal sparse representation of the image in multiple scale and direction, it is a suitable option for extracting important features from an image.

It is observed that LBP and its variant based approaches lack the capacity to capture the very fine details present in images. To deal with this issue, a few techniques based on bit-plane decomposition which captures coarser to very finer image details are proposed[81–84]. With appropriate encoding of these bit-planes, the coarser to very fine information of the images can be extracted for the design of effective biomedical image retrieval strategies.

This chapter introduces following descriptors in the NSST domain for biomedical image retrieval which captures coarse to very fine image information existing in NSST subbands via bit-plane decomposition:-

1. Biomedical image retrieval using local bit-plane based dissimilarities and adder pattern (LBPDAP) in NSST domain (NSST-LBPDAP)

2. Biomedical image retrieval using local bit-plane neighbour dissimilarity pattern in NSST domain (NSST-LBNDP)

4.1 Biomedical image retrieval using local bit-plane based dissimilarities and adder pattern in NSST domain (NSST-LBPDAP)

This section introduces one biomedical image retrieval approach which extends the existing spatial domain LBPDAP [83] scheme in NSST domain. The NSST subband coefficients are not sufficient enough for texture cues, hence the bit-plane decomposition cannot be applied directly to the NSST subbands. The NSST coefficients' sensitivity towards local variations needs to be decreased before bit-plane decomposition. Hence, before extracting features from the subbands, we apply non-linearity followed by smoothing for this purpose. To distinguish between texture patches having the same average brightness and 2^{nd}-order properties, non-linearity is added to the NSST coefficients. After the addition of non-linearity followed by smoothing, the NSST coefficient values are normalized into the range [0-255]. Bit-plane decomposition is then applied to each of the subbands, to obtain eight different bit-plane slices carrying coarser to finer details. In each of these bit-planes, the centre-neighbor and neighbor-neighbor dissimilarity relationships are encoded first and then using a single adder, joint dissimilarity information is obtained. The relationship between this joint dissimilarity information and the normalized local energy estimate in reference position is eventually encoded to produce the LBPDAP in the NSST domain (NSST-LBPDAP).

4.1.1 Methodology

The block diagram of NSST-LBPDAP descriptor in content based biomedical image retrieval framework is demonstrated in Fig. 4.1. The whole procedure of computing NSST-LBPDAP is divided into the following steps: NSST decomposition, non-linearity insertion, decomposition into bit-plane slices, bit-plane encoding in NSST domain using LBPDAP concept and formation of final feature vector.

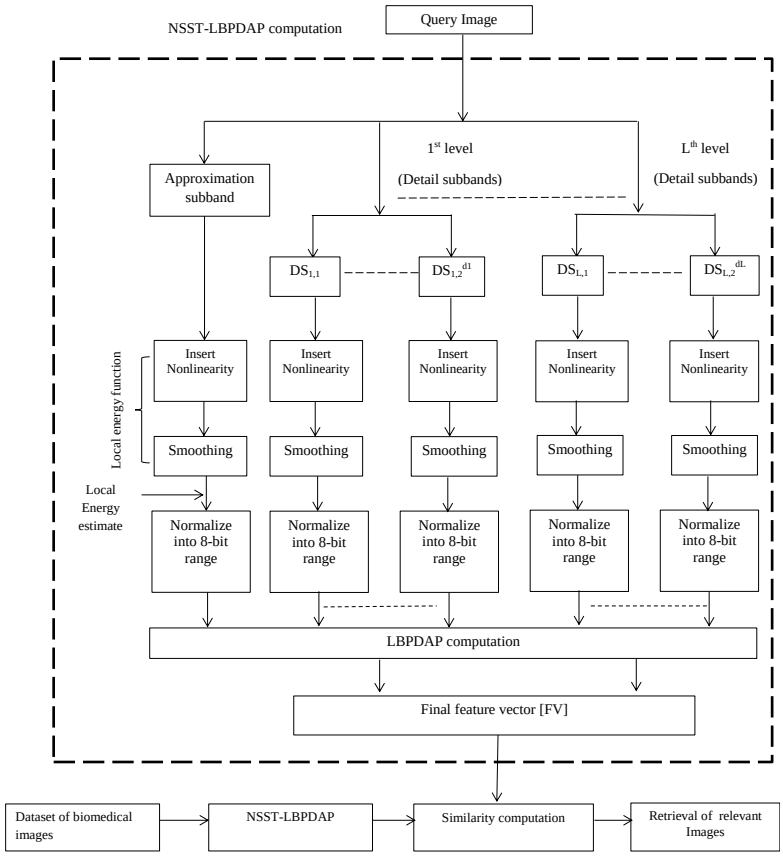

Figure. 4.1: An overview of NSST-LBPDAP based image retrieval system

The brief discussion on NSST is presented in the previous chapter. The remaining steps are discussed in the following subsections.

4.1.2 Incorporation of non-linearity

Image NSST coefficients in their current state are insufficient for texture cues, like wavelet coefficients. The NSST coefficients assist in splitting texture information into various frequencies. Non-linearity is incorporated to distinguish between textural areas of similar mean brightness and 2^{nd}order details.

Before extracting features for texture retrieval, the NSST-LBPDAP descriptor uses non-linearity and smoothing to the NSST coefficients to make them less sensitive to local heterogeneity [196]. Many different types of nonlinearities, including rectified sigmoid and squaring, are used in literature [146]. Smoothing often involves the use of Gaussian or low pass (rectangular) filters. Similar to [146], the NSST-LBPDAP descriptor also combines non-linearity and smoothing into a single operation, which is regarded as advantageous from a computational standpoint. The magnitude of subband coefficients in a 3×3 neighborhood is

squared first, afterwards their mean is computed. The local energy calculation in a 3×3 neighbourhood around one reference image NSST coefficient $x(i, j)$ is given as :

$$E_L(i,j) = \frac{1}{9} \sum_{p1=0}^{2} \sum_{q1=0}^{2} |x(i-1+p1, j-1+q1)|^2 \tag{4.1}$$

To ensure that these energy values fit into a specific dynamic range, they must first be normalized. For bit-plane decomposition to be applied on these local energy values computed through (4.1), the normalization is done next so that they fit into a suitable 8 bit range.

4.1.3 Bit-plane decomposition

In this step, bit-plane decomposition is applied on E_L (with dimension $m \times n$) obtained using (4.1) which results into 8 binary bit-planes with bit depth B:

$$E_L(i,j) = \sum_{b=0}^{B-1} BB_b(i,j) \times 2^b : i \in [1,m], j \in [1,n], b \in [0,7] \tag{4.2}$$

$BB_b(i, j)$ is the binary bit of $E_L(i, j)$ in b^{th} bit-plane.

Bit-plane slicing leads to the generation of eight bit-planes that carry an image's fine to coarse details. The various aspects of an image are characterised by these bit-plane slices. The 8 bit-planes obtained for an image is depicted in Fig. 4.2.

The eight bit-planes produced by bit-plane decomposition on an image from the TCIA-CT database are shown pictorially in Fig. 4.3. The observations from these bit-plane slices indicate the presence of very fine to coarse details in the lower to higher bit-planes.

9	18	71	61	20
23	17	41	91	38
11	15	34	82	25
174	61	14	19	250
13	58	49	118	125

(a)

1	0	1	1	0
1	1	1	1	0
1	1	0	0	1
0	1	0	1	0
1	0	1	0	1

BB_0

0	1	1	0	0
1	0	0	1	1
1	1	1	1	0
1	0	1	1	1
0	1	0	1	0

BB_1

0	0	1	1	1
1	0	0	0	1
0	1	0	0	0
1	1	1	0	0
1	0	0	1	1

BB_2

1	0	0	1	0
0	0	1	1	0
1	1	0	0	1
1	1	1	0	1
1	1	0	0	1

BB_3

0	1	0	1	1
1	1	0	1	0
0	0	0	1	1
0	1	0	1	1
0	1	1	1	1

BB_4

0	0	0	1	0
0	0	1	0	1
0	0	1	0	0
1	1	0	0	1
0	1	1	1	1

BB_5

0	0	1	0	0
0	0	0	1	0
0	0	0	1	0
0	0	0	0	1
0	0	0	1	1

BB_6

0	0	0	0	0
0	0	0	0	0
0	0	0	0	0
1	0	0	0	1
0	0	0	0	0

BB_7

(b)

Figure. 4.2: (a)Example Image (b)The eight bit-planes BB_0(least significant) to BB_7 (most significant)

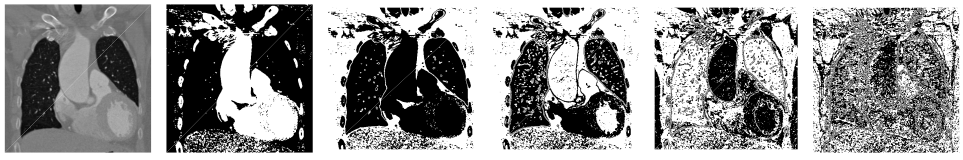

(a) An image from TCIA-CT (b) BB_7 (c) BB_6 (d) BB_5 (e) BB_4 (f) BB_3

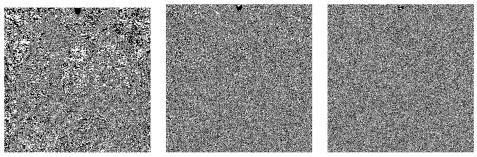

(g) BB_2 (h) BB_1 (i) BB_0

Figure. 4.3: Bit-plane slices of a given image from TCIA-CT dataset after bit-plane decomposition

4.1.4 Local bit-plane based dissimilarities and adder pattern(LBPDAP)

The sample computation of LBPDAP is shown in Fig. 4.4.

LBPDAP considers two different types of dissimilarity: one is centre-neighbor dissimilarity and the other is neighbor-neighbor dissimilarity. The centre-neighbor dissimilarity information is computed as follows-

$$CN_b^T(i,j)|_{b\in[0,7],T\in[1,8]} = D_{is}(BB_b(i,j), BB_b^T(i,j)) \tag{4.3}$$

$$D_{is}(u,v) = \begin{cases} 1 & if u \neq v \\ 0 & else \end{cases} \tag{4.4}$$

In the above two equations, $D_{is}(BB_b(i,j), BB_b^T(i,j))$ signifies the dissimilarity relationship calculated between center bit $BB_b(i,j)$ in b^{th} bit-plane and its neighbors $BB_b^T(i,j), T \in [1,2,..8]$ in local neighborhood with radius $R = 1$. In LBPDAP computation, only the four significant bit-planes $b \in [7,6,5,4]$ are taken into consideration in order to limit the dimensions. Using equation (4.3), the bit-planes BB_7, BB_6, BB_5, BB_4 are transformed into 8 bit binary code as $CN_7^T, CN_6^T, CN_5^T, CN_4^T$.

The dissimilarity between neighbors is calculated in each of the bit-planes, considering each neighbor and its adjacent neighbor (w.r.t one reference/center bit) as follows

$$NN_b^T(i,j)|_{b\in[0,7],T\in[1,8]} = \begin{cases} D_{is}(BB_b^T(i,j), BB_b^{T+1}(i,j)); if T \in [1,7] \\ D_{is}(BB_b^T(i,j), BB_b^1(i,j)); if T = 8 \end{cases} \tag{4.5}$$

where $D_{is}(BB_b^T(i,j), BB_b^{T+1}(i,j))$ is the dissimilarity information computed between neighboring bit $BB_b^T(i,j)$ and its immediate adjacent neighboring bit in clockwise direction $BB_b^{T+1}(i,j)$. The bit-planes $BB_b, b \in [4,5,6,7]$ are converted into 8 bit binary $NN_b^T(i,j), b \in [4,5,6,7], T \in [1,2,3,....8]$.

The two dissimilarity informations $NN_b^T(i,j)|_{b\in[0,7],T\in[1,8]}$ and

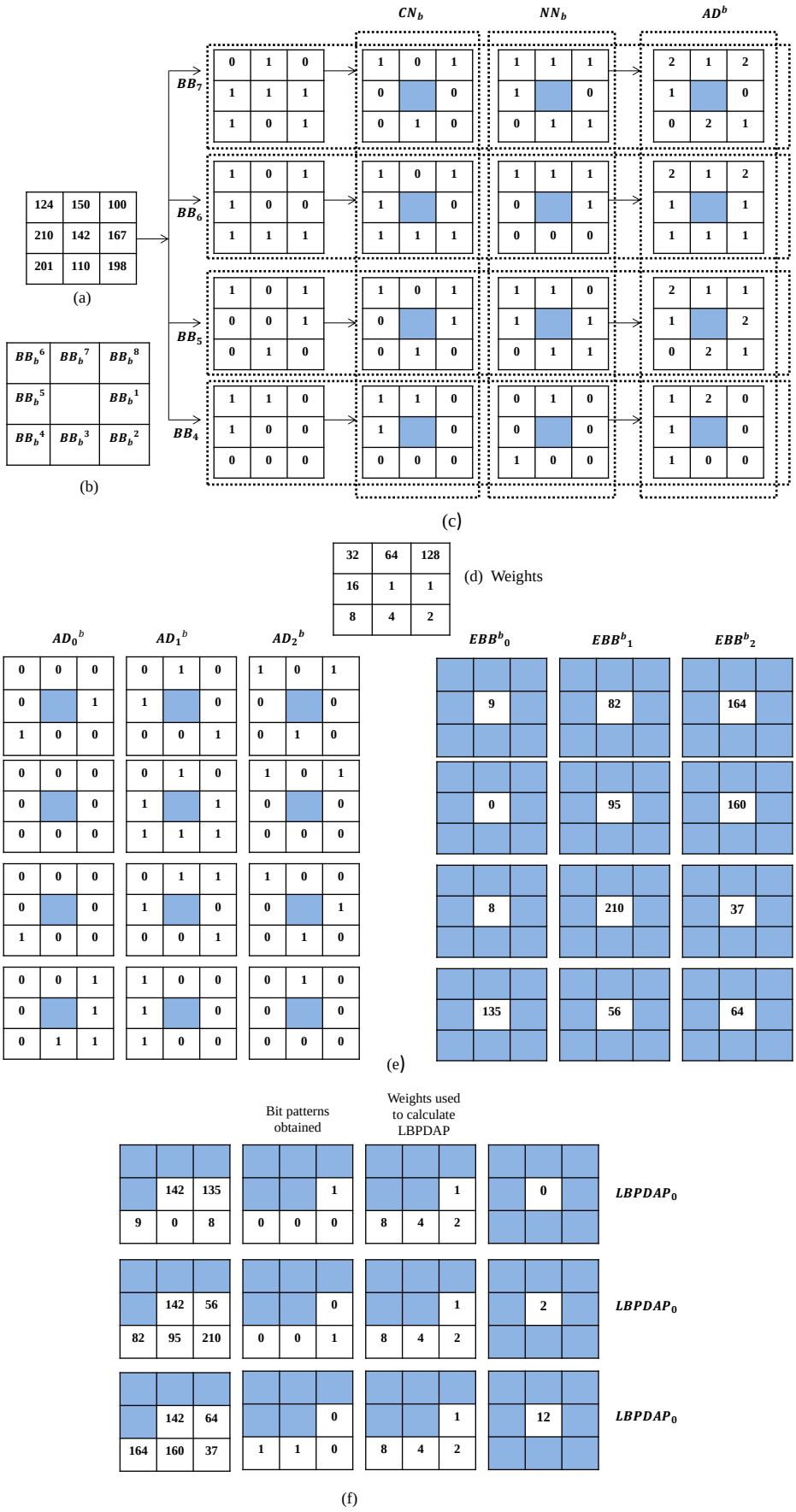

Figure. 4.4: An example computation of LBPDAP (a)Example image, (b)Position of the bit-plane neighbors, (c)Calculation of adder pattern, (d)Weights, (e)Obtained encoded bit-planes and(f)Computation of LBPDAP

$CN_b^T(i,j)|_{b\in[0,7],T\in[1,8]}$ are further encoded with an adder in LBPDAP descriptor. With these two information, the adder pattern AD_b^T is obtained as

$$AD^{T,b}(i,j)|_{b\in[0,7],T\in[1,8]} = CN_b^T(i,j) + NN_b^T(i,j) \tag{4.6}$$

The adder pattern $AD^{T,b}$ consists of three possible values [0,1,2] and are further divided into three different planes $AD_d^{T,b}, d \in [0,1,2]$.

$$AD_d^{T,b}(i,j)|_{b\in[0,7],T\in[1,8],d\in[0,2]} = \begin{cases} 1 & if AD_d^{T,b}(i,j) = d \\ 0 & else \end{cases} \tag{4.7}$$

Each of these three binary bit patterns are then multiplied with corresponding weights and added to obtain EBB_d^b,the encoded bit-plane value. These encoded bit-plane values are in the range [0-255], three different EBB_d^b values are obtained for each reference/centre position.

$$EBB_d^b(i,j) = \sum_{T=1}^{8} 2^{T-1} \times AD_d^{T,b}(i,j) \tag{4.8}$$

Using this encoded bit-plane values, three $LBPDAP_d(i,j)$ values are obtained for the bit-planes considered for a reference/centre position.

$$LBPDAP_d(i,j) = \sum_{b=4}^{7} 2^{b-4} wt(E_L(i,j), EBB_d^b(i,j)) \tag{4.9}$$

$$wt(u,v) = \begin{cases} 1 & if u \leq v \\ 0 & else \end{cases} \tag{4.10}$$

As a result, three $LBPDAP_d, d = [0,1,2]$ pattern maps with values in the range [0-15] are generated. These pattern maps are partitioned into four non overlapping and equal sized sub maps. Histograms of the submaps of these three

pattern maps' are computed to generate the final feature vector.

$$\begin{aligned} FV = [&H_{LBPDAP_0^{s_1}}, H_{LBPDAP_0^{s_2}}, H_{LBPDAP_0^{s_3}}, H_{LBPDAP_0^{s_4}}, \\ &H_{LBPDAP_1^{s_1}}, H_{LBPDAP_1^{s_2}}, H_{LBPDAP_1^{s_3}}, H_{LBPDAP_1^{s_4}}, \\ &H_{LBPDAP_2^{s_1}}, H_{LBPDAP_2^{s_2}}, H_{LBPDAP_2^{s_3}}, H_{LBPDAP_2^{s_4}}] \end{aligned} \tag{4.11}$$

The three pattern maps $LBPDAP_d, d = 0, 1, 2$ have pattern values in the range $[0 - 15]$. As the final histograms are formed from the four non overlapping submaps of these pattern maps, the FV of $LBPDAP$ [83] contains a dimension of size $3 \times 16 \times 4 = 192$.

4.1.5 Construction of final feature vector

Two level NSST in 2,2 directions is used to decompose the input image which results into one approximation and a total of $2^2 + 2^2 = 4 + 4 = 8$ detail subbbands. These subbands are subjected to LBPDAP, and the histograms derived from them are concatenated to form the final feature vector of the NSST-LBPDAP, which has a feature dimension of $9 \times 192 = 1728$.

The algorithm for NSST-LBPDAP based image retrieval framework is presented below:-

---

Algorithm: The biomedical image retrieval approach with NSST-LBPDAP based features.

Require: Input: Query image: Output: n_T number of images retrieved

1. Apply NSST on input image to decompose it into number of subbands
2. Insert non-linearity onto the NSST subbands through equation(4.1) and normalize them to the interval [0,1]. Multiply the normalized values by 255.
3. Apply bit-plane decomposition to output obtained in step 2 via equation (4.2).
4. Consider only four significant bit-planes of the output obtained from step 3

5. Form the final feature vector using equation (4.11) by concatenating the LBPDAP histograms obtained from the NSST subbands
6. Perform similarity measurement using d_1 distance
7. Retrieve n_T number of images

4.1.6 Experimental results and discussion

At the beginning of this section, a discussion on the datasets used for the experiments, followed by a discussion of the performance evaluation metrics used to assess the results are presented. The discussion of the results obtained through experiments conducted on the considered datasets is reported in the later part of this section.

4.1.6.1 Datasets considered

For the experiments, three publicly available datasets are taken into consideration. Out of these three, two are CT image datasets: NEMA-CT [197] and TCIA-CT [198] and one is MRI image dataset: York-MRI [199]. The details about these datasets are presented in the following table:

Table 4.1: Details about datasets considered

Dataset	No. of classes	Total images	Dimension
NEMA-CT [197]	9	315	512×512
TCIA-CT [198]	16	696	512×512
YORK-MRI [7, 199]	4	420	256×256

Fig.s 4.5, 4.6 and 4.7 presents one sample image from each image class of NEMA-CT, TCIA-CT and YORK-MRI dataset.

4.1.6.2 Performance Evaluation Measures

Each image in the database is viewed as a query once during the experiments, and the performance assessment parameters are determined from the respective

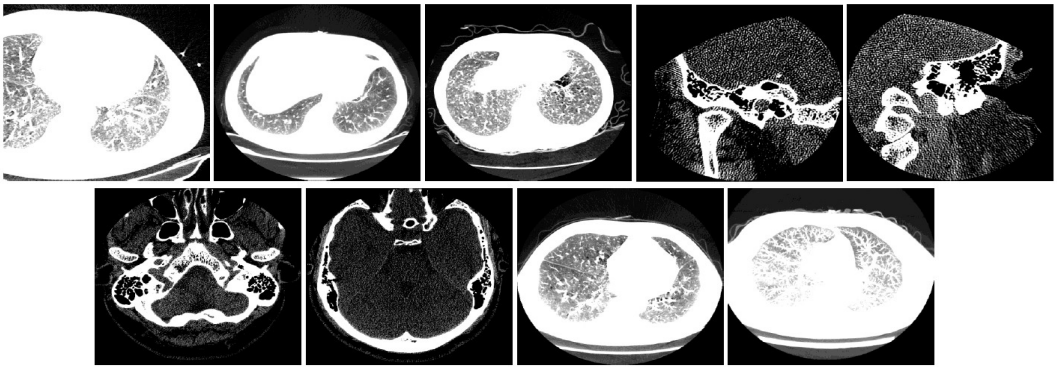

Figure. 4.5: Sample images of different classes of NEMA-CT

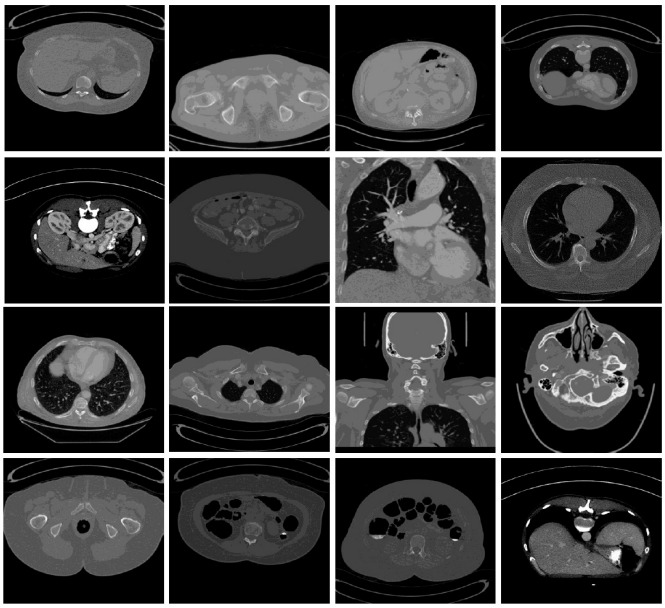

Figure. 4.6: Sample images of different classes of TCIA-CT

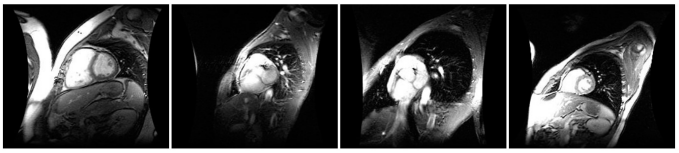

Figure. 4.7: Sample images of different classes of YORK-MRI

retrieval results. We quantify how effectively a retrieval framework works by computing: the average retrieval precision (ARP) and the average retrieval recall (ARR).

For retrieval performance analysis, ARP and ARR parameters are used

here. $\%ARP$ and $\%ARR$ are calculated as follows [84, 200]-

$$ARP = \frac{1}{|TD|}\sum_{k=1}^{|TD|} P(I_k) \times 100 \tag{4.12}$$

$$ARR = \frac{1}{|TD|}\sum_{k=1}^{|TD|} R(I_k) \times 100 \tag{4.13}$$

with TD = entire images available in the dataset.

$$P(I_k) = \frac{\text{Number of images found to be relevant}}{\text{Total number of images retrieved}} \tag{4.14}$$

$$R(I_k) = \frac{\text{Number of images found to be relevant}}{\text{Total relevant images present in database}} \tag{4.15}$$

4.1.6.3 Experimental results obtained for considered datasets

For the experiments conducted on NEMA-CT database, to obtain and plot the %ARP and %ARR values, the images are retrieved for top match of 10,15,20,25,30 number of images. Table 4.2 presents the % ARP and % ARR values obtained for the NEMA-CT for 30 no. of uppermost matches. The Fig. 4.8(a-b) presents the plot of %ARP and % ARR for different top matches. From the Table 4.2 and Fig. 4.8(a-b), the following points can be noted.

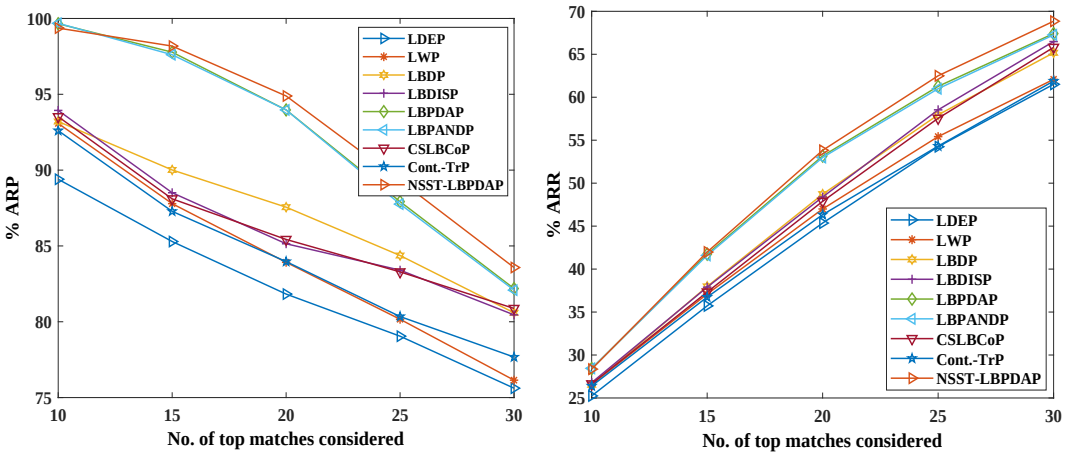

(a) (b)

Figure. 4.8: Comparison of NSST-LBPDAP with other schemes for NEMA-CT

Table 4.2: Evaluation of the NSST-LBPDAP descriptor against other approaches for the NEMA-CT dataset, comparing their % ARP and % ARR values (Top 30 match)

Method	LDEP[200]	LWP[201]	LBDP[81]	LBDISP[82]	LBPDAP[83]	LBPANDP[84]	CSLBCOP[114]	Cont.-TrP[202]	NSST-LBPDAP
ARP	75.61	76.14	80.59	80.45	82.19	82.08	80.87	77.25	**83.57**
ARR	61.50	62.80	65.17	66.48	67.40	67.25	65.80	61.52	**68.84**

1. From the curve, presented in Fig. 4.8(a), it is observed that, NSST-LBPDAP shows consistent improvement upon other existing approaches for top match 15 and above. However for lower top matches, the NSST-LBPDAP shows a little inferior % ARP value compared to LBPDAP and LBPANDP descriptors. It is observed from the Fig. 4.8(b), that NSST-LBPDAP achieves competitive results with spatial LBPDAP which further provides motivation to develop effective local bit-plane based descriptors in NSST domain.

2. From Table 4.2 it is clearly visible that the NSST-LBPDAP for 30 top matches surpasses the existing relevant techniques: LDEP [200], LWP [201], LBDP [81], LBDISP [82], LBPDAP [83], LBPANDP [84], CSLBCOP [114] and Cont.-TrP [202]. In terms of %ARP, NSST-LBPDAP for 30 top matches outperforms other bit-plane based feature descriptors LBDP, LBDISP, LBPDAP and LBPANDP by 3.70%, 3.88%, 1.68%, 1.82% respectively. NSST-LBPDAP also shows 10.5277%, 9.76%, 3.34% and 8.18% improvement over LDEP, LWP, CSLBCOP and Cont.-TrP descriptors respectively.

3. However in terms of % ARR, NSST-LBPDAP shows improvement of 9.62%, 11.94%, 3.55%, 5.63%, 2.36%, 2.14%, 4.62% and 11.89% over LWP, LDEP, LBDISP, LBDP, LBPANDP, LBPDAP, CSLBCOP and Cont.-TrP respectively.

Table 4.3: Evaluation of the NSST-LBPDAP descriptor against other approaches for the TCIA-CT dataset, comparing their % ARP and % ARR values (Top 30 match)

Method	LDEP[200]	LWP[201]	LBDP[81]	LBDISP[82]	LBPDAP[83]	LBPANDP[84]	CSLBCOP[114]	Cont.-TrP[202]	NSST-LBPDAP
ARP	73.48	75.36	81.95	89.72	91.71	90.61	75.78	89.00	**92.74**
ARR	52.47	54.05	57.05	60.87	62.37	61.68	53.82	61.70	**62.46**

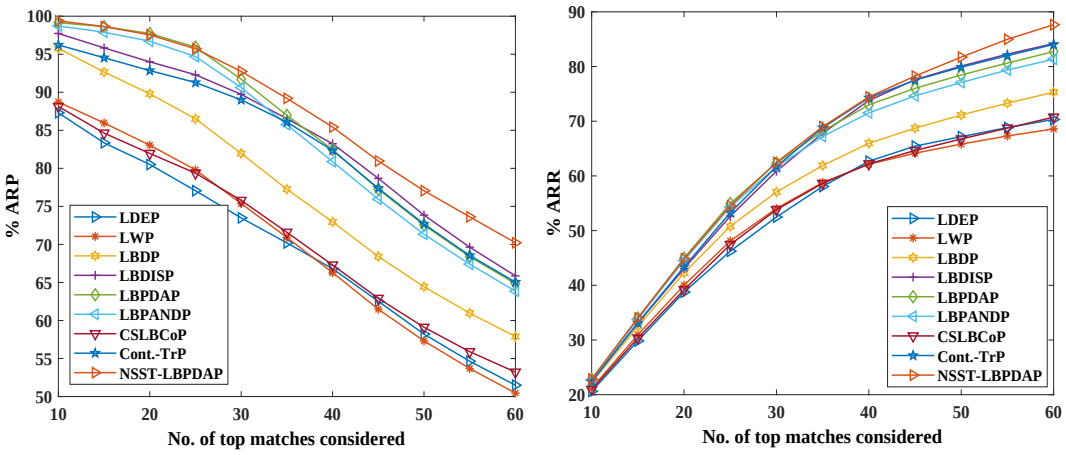

(a) (b)

Figure. 4.9: Comparison of NSST-LBPDAP with other schemes for TCIA-CT

For TCIA-CT dataset, the experimental results obtained in terms of % ARP and % ARR, are presented in the Table 4.3 and the values obtained for top match of 10, 15, 20, ...,60 number of images are plotted in Fig. 4.9(a-b). The observations obtained from the table and curves are reported below.

1. From the %ARP and %ARR plot for top match of 10, 15, 20,...60 number of images presented in Fig. 4.9(a-b), it is observed that the NSST-LBPDAP shows consistently superior results to all the approaches however the NSST-LBPDAP performs close to spatial LBPDAP till 25 number of top matches.

2. The NSST-LBPDAP outperforms LDEP, LWP, LBDP, LBDISP, LBP-DAP, LBPANDP, CSLBCOP and Cont.-TrP in terms of [ARP,ARR]% by [26.21,19.04]%, [23.06, 15.56]%, [13.17,9.48]%, [3.37,2.61]%, [1.12,0.1441]%, [2.35,1.26]% and [22.38,16.05]% respectively for 30 top matches

3. For TCIA-CT too, the NSST-LBPDAP performs consistently superior than spatial LBPDAP at top matches greater than 25 and above.

For the experiments performed on YORK-MRI dataset, the results obtained are presented in Table 4.4 and Fig.s 4.10(a-b). For evaluation, images are retrieved for different top match of images and the resultant % ARP and % ARR values are plotted. From Table 4.4 and Fig. 4.10(a-b), the following points can be observed.

1. The %ARP and % ARR curves in Fig. 4.10(a-b) depicts that the performance of NSST-LBPDAP is better than all other approaches consistently

except for LBDP scheme where the NSST-LBPDAP performs too close to LBDP till top match of 50 after which it outperforms LBDP too.

2. The Table 4.4 contains the %ARP and %ARR values obtained for top match of 100 images. It is observed that NSST-LBPDAP achieves [39.32%, 9.33%, 10.88%, 0.90%, 25.15%, 19.39%, 9.05%, 11.25%] and [41.99%, 10.22%, 11.31%, 0.92%, 24.27%, 18.33 %, 8.99%, 12.49%] improvement over existing schemes like LWP, LDEP, LBDISP, LBDP, LBPANDP, LBPDAP, CSLBCOP and Cont.-TrP respectively in terms of %ARP and % ARR.

Table 4.4: Evaluation of the NSST-LBPDAP descriptor against other approaches for the YORK-MRI dataset, comparing their % ARP and % ARR values (Top 100 match)

Method	LDEP[200]	LWP[201]	LBDP[81]	LBDISP[82]	LBPDAP[83]	LBPANDP[84]	CSLBCOP[114]	Cont.-TrP[202]	NSST-LBPDAP
ARP	84.42	66.25	91.47	83.24	77.31	73.75	84.64	82.96	**92.30**
ARR	79.15	61.44	86.44	78.37	73.72	70.20	80.04	77.55	**87.24**

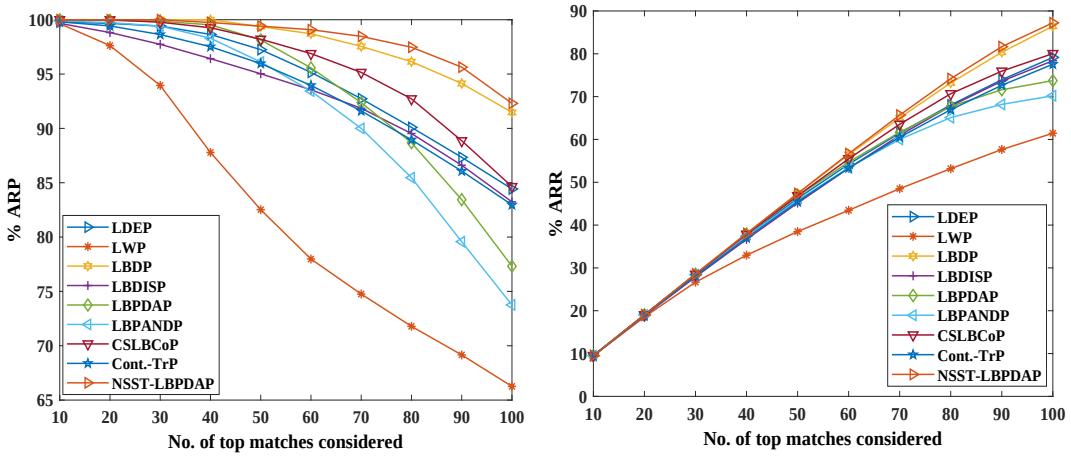

(a) (b)

Figure. 4.10: Comparison of NSST-LBPDAP with other schemes for YORK-MRI

Table 4.5 tabulates the performance obtained for NSST-LBPDAP, considering different directions and scales for YORK-MRI. With increase in number of scale of decomposition, it is seen that the retrieval performance increases too with increase in feature dimension size. Again, the performance also depends upon number of directions considered in different scales of NSST decomposition. In order to maintain a practical balance of retrieval performance and feature dimension size, the level of NSST decomposition is set to two with [2,2] number of directions for construction of feature descriptor for NSST-LBPDAP.

Table 4.5: Evaluation of the NSST-LBPDAP descriptor against other approaches for YORK-MRI dataset (top match 100) for various NSST decomposition levels and directions in terms of % ARP and % ARR

Level	Direction	Total no. of subbands	NSST-LBPDAP		FD
			ARP	ARR	
1	2	1+4=5	90.92	86.12	960
	3	1+8=9	91.18	86.36	1728
	4	1+16=17	91.48	86.61	3264
	5	1+32=33	92.09	87.14	6336
2	2 2	1+4+4=9	92.30	87.24	1728
	3 3	1+8+8=17	92.57	87.70	3264
	4 4	1+16+16=33	92.21	87.38	6336
	5 5	1+32+32=65	92.16	78.42	12480
3	2 2 2	1+4+4+4=13	92.84	88.06	2496
	3 3 3	1+8+8+8=25	92.59	87.77	4800
	4 4 4	1+16+16+16=49	92.30	87.57	9408
	5 5 5	1+32+32+32=97	92.27	87.57	18624

Table 4.6 depicts the dimension of various feature descriptors including NSST-LBPDAP. It possess comparatively higher dimension than LWP, LDEP, LBDISP, LBDP, LBPANDP, LBPDAP, CSLBCOP and Cont-TrP.

Table 4.6: Comparison of feature descriptor size of NSST-LBPDAP with other descriptors

Method	LDEP[200]	LWP[201]	LBDP[81]	LBDISP[82]	LBPDAP[83]	LBPANDP[84]	CSLBCOP[114]	Cont.-TrP[202]	NSST-LBPDAP
Dimension	24	256	256	256	192	64	1024	1475	1728

In Table 4.7, the total retrieval time(in seconds) for different techniques are tabulated. The retrieval time (in sec) for a particular database is computed by estimating the total time required to match the query image with each image in the dataset, with feature dimensions playing a significant role. The total retrieval time plays more important role than feature extraction time in a practical CBIR system [81]. When the database sizes are huge, the role of total retrieval time becomes more crucial. The total retrieval time of NSST-LBPDAP is inferior to other approaches, as it posses highest feature dimension compared to others.

In Fig. 4.11, the top 10 retrieved images for one query image from NEMA-CT dataset, for various descriptors is presented. The NSST-LBPDAP descriptor is seen to retrieve most relevant images more accurately than other strategies. This visual result validates the superiority of NSST-LBPDAP over existing descriptors for retrieval purposes.

Table 4.7: Evaluation of the NSST-LBPDAP descriptor against other approaches in terms of total retrieval time (seconds)

Method	LDEP[200]	LWP[201]	LBDP[81]	LBDISP[82]	LBPDAP[83]	LBPANDP[84]	CSLBCOP[114]	Cont.-TrP[202]	NSST-LBPDAP
NEMA-CT	0.10	0.24	0.26	0.28	0.21	0.18	0.78	1.61	2.34
TCIA-CT	0.46	1.21	1.01	1.27	1.07	0.56	3.50	8.49	16.96
YORK-MRI	0.37	0.63	0.62	0.53	0.45	0.35	1.26	3.11	3.52

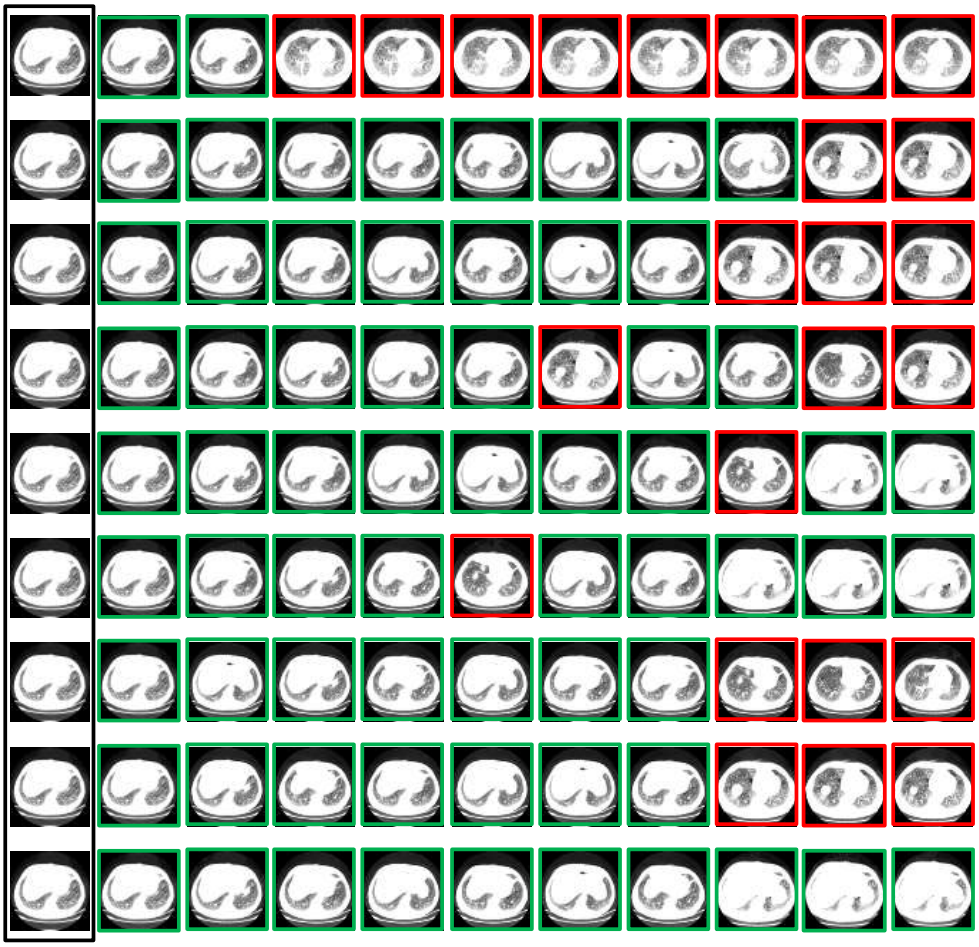

Figure. 4.11: The retrieved images for LDEP, LWP, LBDP, LBDISP, LBPDAP, LBPANDP, CSLBCoP, Cont.-TrP, and NSST-LBPDAP techniques for one sample query image (for top ten image matches),(The image in the black box is a query image; the images in the green boxes were correctly retrieved; the images in the red boxes were incorrectly retrieved.))

The comparison of bit-plane based approaches, including LBDP, LBPDAP, LBDISP, LBPANDP, and NSST-LBPDAP with intra class and inter class example images are shown in Fig. 4.12. I1, I2 and I3, these three images belong to TCIA-CT dataset, out of which I1 and I2 are from same image class and I3 is taken from

a different image class. The Fig. 4.12(d-e) displays the probability distribution of various descriptors when comparing the feature vector differences between images I1-I2 (same class) and I2-I3 (different class) and taking into account a zero mean. High variance relative to the zero mean implies less similarity between the feature vectors, but high amplitude relative to the zero mean demonstrates high similarity. Fig. 4.12(d-e) shows the superior discriminative power of NSST-LBPDAP features by matching intraclass images and discriminating interclass images.

The successful extension of existing LBPDAP to NSST-LBPDAP shows an encouraging concept of implementing local bit-plane based scheme in NSST domain. By adopting powerful encoding strategies the total retrieval time and these descriptors' retrieval performance can be improved.

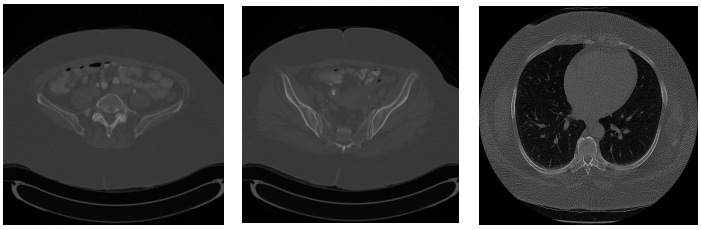

(a) I1 (b) I2 (c) I3

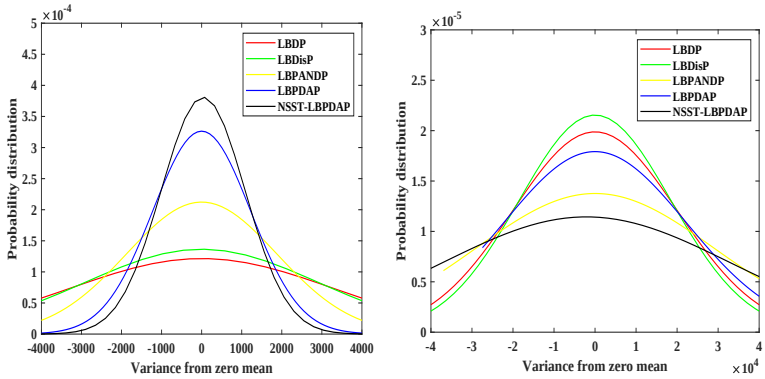

(d) Probability distribution(p.d) of feature vector difference(I1-I2) of intraclass images for different descriptors

(e) p.d of feature vector difference(I2-I3) of interclass images for different descriptors

Figure. 4.12: The illustration of distinguishing conduct of LBPDAP, LBDP, LBPANDP, LBDISP and NSST-LBPDAP features in discriminating interclass and intraclass images belonging to TCIA-CT

4.2 Local bit-plane neighbour dissimilarity pattern in NSST domain for bio-medical image retrieval (NSST-LBNDP)

This section introduces one content based biomedical image retrieval approach via local bit-plane neighbour dissimilarity pattern in NSST domain known as NSST-LBNDP. The input image is decomposed with NSST first and then non-linearity is inserted onto the NSST subbands as described in the previous subsection. Normalization is then carried out as described in the previous subsection in order to generate eight-bit values. These eight bit values of NSST subbands are further decomposed into eight bit-planes through bit-plane slicing. The bit-planes in the NSST-LBPDAP descriptor are encoded by taking into account the dissimilarity between each neighboring bit and its adjacent neighbors. This descriptor unlike LBPDAP technique encodes all the bit-planes in order to include more fine details. In the NSST-LBNDP technique, unlike other relevant methods, the relationship between all the encoded bit-plane values and the corresponding reference local energy feature value is computed for each local reference.

4.2.1 Methodology

In this approach, the input image is first decomposed into one approximation subband and several detail subbands using NSST. A brief discussion on NSST is presented in the previous chapter. These NSST subbands are further processed by incorporating non-linearities and converting into 8 bit values by normalization discussed in the previous section.The NSST-LBNDP, encodes each bit-plane created from the NSST subbands by comparing the dissimilarity between each neighboring bit and its adjacent neighboring bits in relation to a reference point.

The NSST-LBNDP in image retrieval framework's overall block diagram is shown in Fig. 4.13.

Each bit serves as the center or reference for the transformation of the local circular neighborhoods in each bit plane into the encoded bit planes $EB_b, b \in [0, 7]$. While computing EB_b, each neighboring value's (relative to a reference) dissimilarity from its adjacent neighbors is taken into consideration.

The dissimilarity bit or information derived between each neighbor $BB_b^a(i, j)(a \in [1, 8], b \in [0, 7])$ (w.r.t. the center/reference bit $BB_b(i, j)$) and

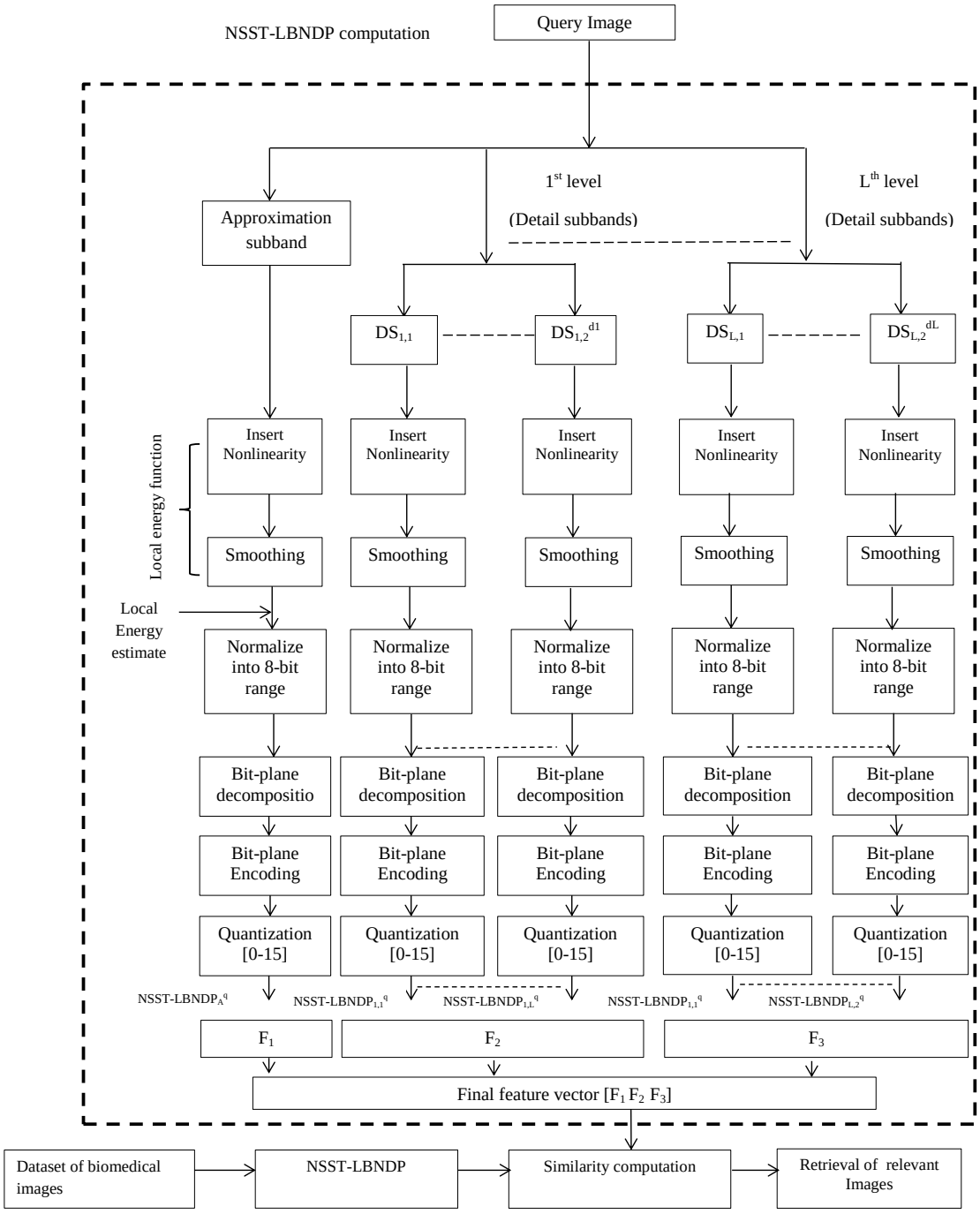

Figure. 4.13: An overview of NSST-LBNDP based image retrieval system

its 8 adjacent neighbors $BB_b^{a,t}(i,j)(t \in [1,8])$ in each k^{th} subband ($k \in [1, N_s]$) are computed in (4.16).

$$[D_{b,k}^{a,t}(i,j)] = \eta(BB_{b,k}^{a}(i,j), BB_{b,k}^{a,t}(i,j)); \quad b \in [0,7], a \in [1,8], t \in [1,8], k \in [1, N_s] \tag{4.16}$$

where $\eta BB^{a}_{b,k}(i,j), BB^{a,t}_{b,k}(i,j))$ is the dissimilarity relationship calculated between $BB^{a}_{b,k}(i,j)$ and $BB^{a,t}_{b,k}(i,j)$ and is given by equation (4.17).

$$\eta(u,v) = \begin{cases} 1, & if \quad u \neq v \\ 0, & else \end{cases} \tag{4.17}$$

The 8 dissimilarity bits obtained using equation (4.16) are merged by summing them together for each k^{th} subband and neighborhood location $a \in [1,8]$ (w.r.t the reference/centre location $BB_b(i,j)$) using the operation in equation (4.18).

$$\zeta^{a}_{b,k}(i,j) = \sum_{t=1}^{8} D^{a,t}_{b,k}(i,j), \quad a \in [1,8] \tag{4.18}$$

An encoded bit-plane value is produced for each bit-plane ($b \in [0,7]$) by thresholding the $\zeta^{a}_{b,k}(i,j)$ value acquired for each neighbor ($BB^{a}_{b,k}(i,j) \quad a \in [1,8]$) around the center/reference ($BB_b(i,j)$) with a threshold T_h and further multiplying with appropriate weights.

$$EB_{b,k}(i,j) = \sum_{a,n=1}^{8} 2^{n-1}\gamma(\zeta^{a}_{b,k}(i,j), T_h), \quad a \in [1,8] \tag{4.19}$$

where

$$\gamma(u,v) = \begin{cases} 1, & if \quad u \geq v \\ 0, & else \end{cases} \tag{4.20}$$

For each k^{th} subband, the encoded bit-plane value $EB_{b,k}(i,j)$ (for each reference/center $BB_{b,k}(i,j)$) ranges between [0 255].

The computation for the lowest bit-plane of the k^{th} NSST subband of a sample image, $(EB_{b,k}(i,j)|_{b=0}$, is illustrated in Fig. 4.14.

By using empirical study, the threshold (T_h) value is set to 4. The encoded bit-plane values of all 8 bit-planes $EB_{b,k}(i,j) \quad (b \in [0,7])$ are compared with the corresponding reference local energy feature value for each reference (i,j) in a k^{th} subband. This comparison is done as shown in Fig. 4.14. Then, the respective weights are multiplied with the corresponding binary outputs to produce the final NSST-LBNDP value.

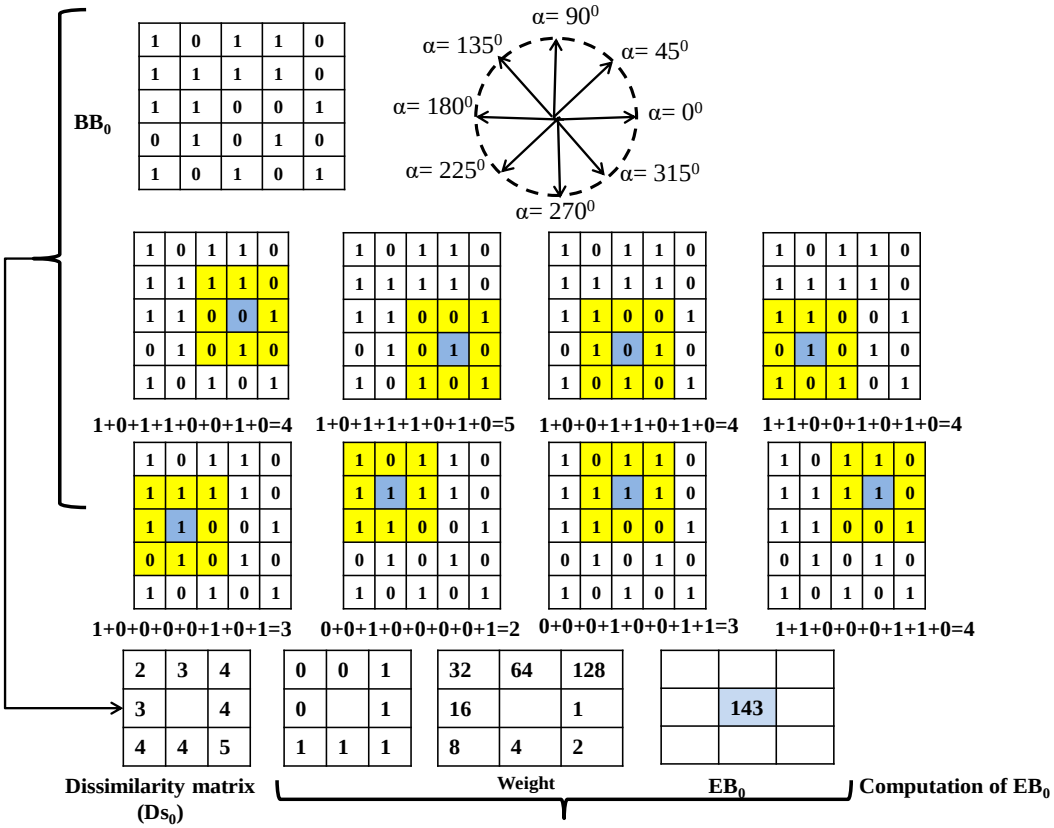

(a) Computation of EB_0 for bit-plane 0 (BB_0)(example)

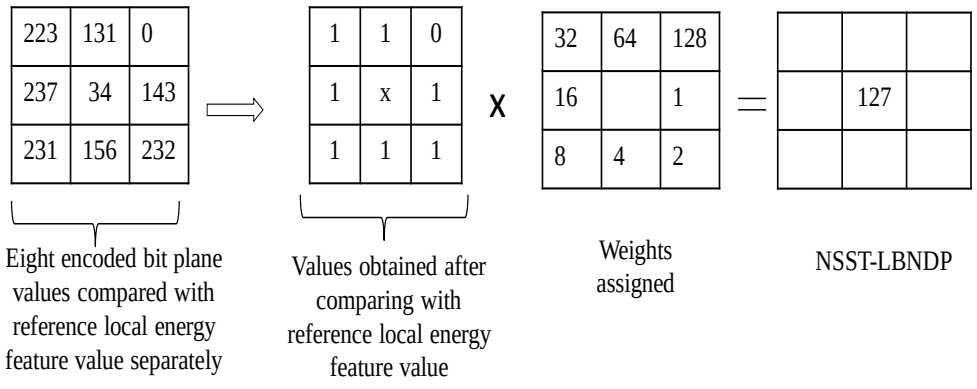

(b) Calculation of $NSST - LBNDP$ from EB_0, EB_1, EB_2, EB_3, EB_4, EB_5, EB_6 and EB_7

Figure. 4.14: Bit-plane encoding of a sample image

$$NSST - LBNDP_k(i,j) = \sum_{b=0}^{7} 2^b \gamma(EB_{b,k}(i,j), E_f(i,j)) \tag{4.21}$$

where $E_{f.k}(i,j)$ is the local energy feature value at $(i,j)^{th}$ location in k^{th} subband.

Similarly, one NSST-LBNDP feature map is constructed for each subband, with values ranging between [0,255]. By employing 2-level NSST with 2, 2 directions to decompose the input image, one approximation and 4+4=8 detail subbands are achieved. If the NSST-LBNDP is used to encode each subband, we get a feature vector of $9 \times 256 = 2304$ elements. In order to restrict the dimension of the feature vector, we quantize each NSST-LBNDP feature map into the interval [0, 15] using the equation (4.22):

$$NSST - LBNDP_k^q(i,j) = round(\frac{15}{255}(NSST - LBNDP_k(i,j))), \quad k \in [1, N_s] \tag{4.22}$$

The feature length of 9 subbands would be $9 \times 16 = 144$ after quantizing the feature maps into the [0 15] range.

4.2.2 Feature vector formation

Every quantized pattern map generated from the NSST subband of an image is divided into 4 same-sized patches. Finally, the computed histograms of each patch are concatenated to generate the final feature vector. The final feature vector is computed using (4.23).

$$FV = \left[H_{NSST-LBNDP^q_{k,s_1}}, H_{NSST-LBNDP^q_{k,s_2}}, H_{NSST-LBNDP^q_{k,s_3}}, H_{NSST-LBNDP^q_{k,s_4}}\right] \tag{4.23}$$

where $k \in [1, N_s]$ and $H_{NSST-LBNDP^q_{k,s_1}}$, $H_{NSST-LBNDP^q_{k,s_2}}$, $H_{NSST-LBNDP^q_{k,s_3}}$ and $H_{NSST-LBNDP^q_{k,s_4}}$ denotes the histogram of the $1^{st}, 2^{nd}, 3^{rd}$, and 4^{th} patches, and N_s the total number of subbands.

When employing two-level NSST with [2, 2] directions, a total of 8 detail subbands and 1 approximation subband are generated. Each of these subbands will generate a quantized feature map using the proposed NSST-LBNDP. By splitting

each of these feature maps into 4 same-sized patches and then forming the feature vector according to equation (4.23), a total of 576 features are obtained. The total feature dimension is calculated by multiplying the number of patches (4), the number of subbands (9) and the number of features per patch (16).

The following is the algorithm for the NSST-LBNDP feature extraction technique:

Algorithm: The algorithm of biomedical image retrieval with the proposed NSST-LBNDP

Require: Input: Query image; Output: n_T‘ number of images retrieved.

1. Decompose the input image using NSST
2. Compute local energy in the NSST subbands obtained through Step 1, using(4.1)
3. Incorporate non-linearity and normalize into the range of [0,1]. Multiply 255 with the normalized values.
4. Obtain bit-plane slices after applying bit-plane decomposition on these 8 bit values of NSST subbands.
5. Encode each bit-plane value $BB_{b,k}(i,j)$ into a $EB_{b,k}(i,j)$ value that ranges between [0, 255] using equations (4.16-4.20)in each bit-plane slice (of k^{th} subband),
6. Using equation (4.21), compare the encoded bit-plane values $EB_{b,k}(i,j)$ for each of the 8 bit-planes at the reference location (i,j), to the corresponding local energy feature value at (i,j) location (achieved from Step2).
7. Multiply the binary comparison outputs generated using equation (4.21) to corresponding weights in order to construct $NSST-LBNDP_k(i,j)$ feature map where the value ranges between [0,255].
8. Quantize the output of Step 7 into a range of [0,15] to form $NSST-LBNDP_k^q(i,j)$ pattern map.
9. Final feature vector is constructed using the $NSST-LBNDP_k^q$ pattern maps by using equation (4.23).
10. Compute similarity measurement using d_1 distance

11. Retrieve n_T number of images

4.2.3 Experimental results obtained for considered datasets

To verify the effectiveness of the proposed NSST-LBNDP, it is compared to a number of popular schemes, which includes a few latest and related schemes like LWP ([200]), LDEP ([200]), LBDISP ([82]), LBDP ([82]), LBPANDP ([84]), LBPDAP ([82]), CSLBCoP[114] and Cont.-TrP [202].

In Table (4.8) and Fig. (4.15(a-b)), the experimental results obtained using the NEMA-CT dataset are displayed. The retrieval results for the top 30 matches in the NEMA-CT database are shown in Table 4.8 in terms of % ARP and % ARR. It is observed that the findings from other approaches, such as LWP, LDEP, LBDISP, LBDP, LBPANDP, LBPDAP, CSLBCoP, and Cont.-TrP, are clearly outperformed by NSST-LBNDP. The proposed scheme performs superior to existing bit-plane-based approaches by a significant margin.

Plots of the $\%ARP$ and $\%ARR$ results for the 10, 15, 20,... 30 best matches are shown in 4.15(a)-(b). The plot clearly illustrates that the proposed NSST-LBNDP outperforms the other techniques in terms of performance. Despite having a lesser feature dimension than CSLBCoP, the NSST-LBNDP consistently outperforms it by a wide margin. In terms of $\%ARP$, the NSST-LBNDP outperforms the LWP, LDEP, LBDISP, LBDP, LBPDAP, LBPANDP, CSLBCoP, and Cont.-TrP by $10.57\%, 11.34\%, 4.64\%, 4.46\%, 2.43\%, 2.57\%, 4.11\%$, and 8.98% for the top 30 matches respectively.

Table 4.8: Comparative performance evaluation of NSST-LBNDP and other approaches in terms of % ARP and % ARR for the NEMA-CT dataset (Top 30 match)

Method	LDEP[200]	LWP[201]	LBDP[81]	LBDISP[82]	LBPDAP[83]	LBPANDP[84]	CSLBCOP[114]	Cont.-TrP[202]	NSST-LBNDP
ARP	75.61	76.14	80.59	80.45	82.19	82.08	80.87	77.25	**84.19**
ARR	61.50	62.80	65.17	66.48	67.40	67.25	65.80	61.52	**69.32**

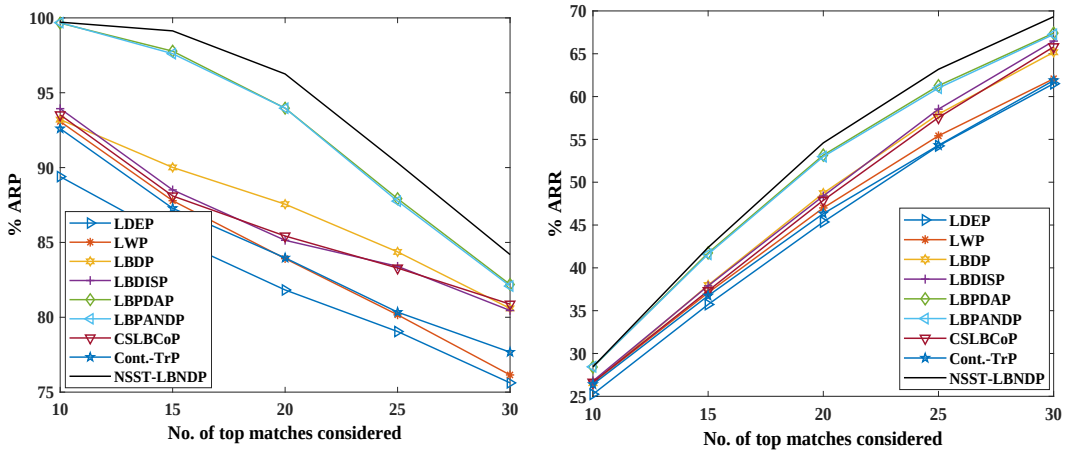

(a) (b)

Figure. 4.15: % ARP and %ARR comparison for NEMA-CT

The performance assessment of the NSST-LBNDP descriptor in terms of $\%ARP$ and $\%ARR$ for the top 30 matches of the TCIA-CT dataset is shown in Table 4.9. In terms of both $\%ARP$ and $\%ARR$, NSST-LBNDP performs superior to the other techniques for the TCIA-CT dataset. The $\%ARP$ and $\%ARR$ computed for different top matches such as 10, 15, 20,....100 are shown in 4.16(a)-(b). These figures clearly demonstrate that the NSST-LBNDP is capable of outperforming the other approaches.In terms of $\%ARP$ and $\%ARR$, the experimental results also demonstrate that the NSST-LBNDP performs better than the other bit-plane-based techniques. The NSST-LBNDP performs better than LWP, LDEP, LBDISP, LBDP, LBPDAP, LBPANDP, CSLBCoP, and Cont.-TrP in terms of $\%ARP$ for the top match of 30, outperforming them by 24.74%, 27.93%, 4.78%, 14.71%, 2.51%, 3.75%, 24.05%, and 5.63%, respectively.

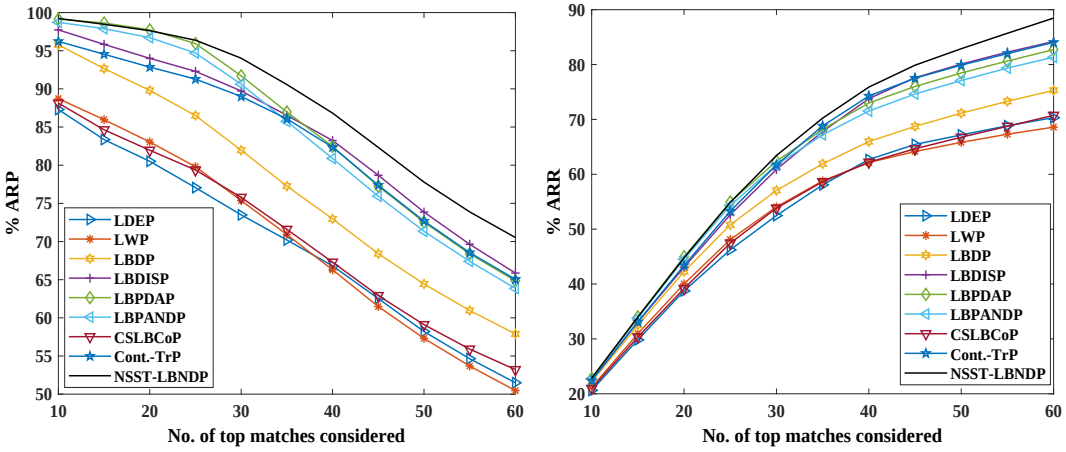

(a) (b)

Figure. 4.16: % ARP and %ARR comparison for TCIA-CT

Table 4.9: Comparative performance evaluation of NSST-LBNDP and other approaches in terms of % ARP and % ARR for the TCIA-CT dataset (Top 30 match)

Method	LDEP[200]	LWP[201]	LBDP[81]	LBDISP[82]	LBPDAP[83]	LBPANDP[84]	CSLBCOP[114]	Cont.-TrP[202]	NSST-LBNDP
ARP	73.48	75.36	81.95	89.72	91.71	90.61	75.78	89.00	**94.01**
ARR	52.47	54.05	57.05	60.87	62.37	61.68	53.82	61.70	**63.42**

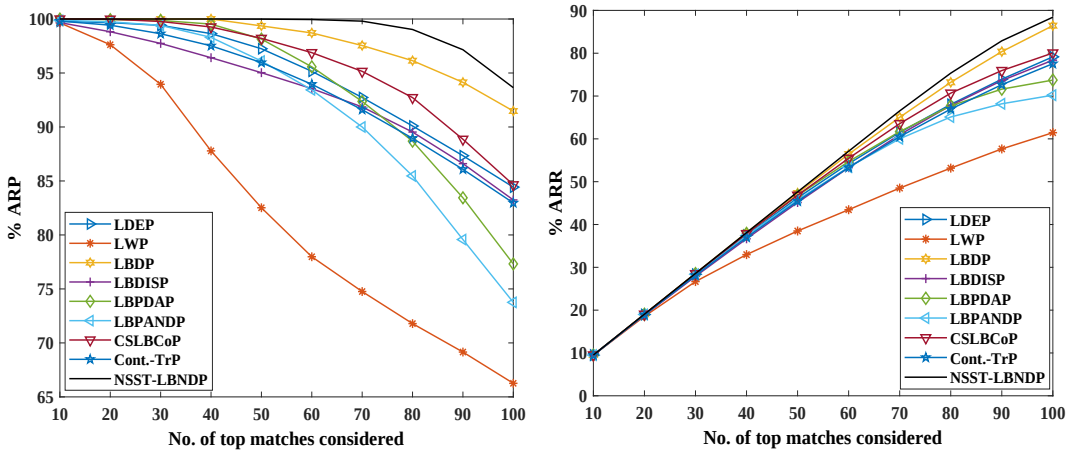

(a) (b)

Figure. 4.17: % ARP and %ARR comparison for YORK-MRI

Table 4.10: Comparative performance evaluation of NSST-LBNDP and other approaches in terms of % ARP and % ARR for the YORK-MRI dataset(Top 100 match)

Method	LDEP[200]	LWP[201]	LBDP[81]	LBDISP[82]	LBPDAP[83]	LBPANDP[84]	CSLBCOP[114]	Cont.-TrP[202]	NSST-LBNDP
ARP	84.42	66.25	91.47	83.24	77.31	73.75	84.64	82.96	**93.64**
ARR	79.15	61.44	86.44	78.37	73.72	70.20	80.04	77.55	**88.41**

Table 4.10 tabulates the performance results for the YORK-MRI dataset in terms of $\%ARP$ and $\%ARR$, and Fig. 4.17(a)-(b) displays the plots for ARP and ARR at the top 10,15,20,....100 matches . Table 4.10 and Fig. 4.17(a)-(b) clearly show that the NSST-LBNDP outperforms the other techniques taken for comparison. The NSST-LBNDP consistently performs with superiority over the other existing bit-plane based descriptors in YORK-MRI, as it does in NEMA-CT and TCIA-CT. In terms of $\%ARP$, the NSST-LBNDP performs

Table 4.11: Comparative performance evaluation of NSST-LBNDP for the YORK-MRI dataset (top match 100) using % ARP and % ARR for various NSST decomposition levels and directions.

Level	Direction	Total no. of subbands	NSST-LBNDP		FD
			ARP	ARR	
1	2	1+4=5	89.22	84.10	320
	3	1+8=9	92.47	87.19	576
	4	1+16=17	92.07	86.83	1088
	5	1+32=33	91.74	86.52	2112
2	2 2	1+4+4=9	93.64	88.41	576
	3 3	1+8+8=17	93.69	88.52	1088
	4 4	1+16+16=33	93.19	88.04	2112
	5 5	1+32+32=65	92.88	87.88	4160
3	2 2 2	1+4+4+4=13	93.77	88.68	832
	3 3 3	1+8+8+8=25	93.40	88.40	1600
	4 4 4	1+16+16+16=49	93.23	88.27	3136
	5 5 5	1+32+32+32=97	93.06	87.13	6208

Table 4.12: Comparison of feature descriptor size of the NSST-LBNDP with other techniques

Method	LDEP[200]	LWP[201]	LBDP[81]	LBDISP[82]	LBPDAP[83]	LBPANDP[84]	CSLBCOP[114]	Cont.-TrP[202]	NSST-LBNDP
Dimension	24	256	256	256	192	64	1024	1475	576

$41.34\%, 10.92\%, 12.49\%, 2.37\%$, $26.96\%, 21.12\%, 10.63\%, 12.87\%$ better than the LWP, LDEP, LBDISP, LBDP, LBPANDP, LBPDAP, CSLBCoP, and Cont.-TrP for top matches of 100 respectively.

The performance of NSST-LBNDP is demonstrated in for various NSST decomposition levels and directions in Table 4.11. We set the NSST decomposition levels to 2 with 2,2 directions due to the trade-off between feature dimensions and retrieval performance.

Table 4.12 compares the feature size of NSST-LBNDP to that of other descriptors. Despite having a greater feature size than LDEP, LWP, LBDP, LBDISP, LBPDAP, LBPANDP, and a considerably lower dimension than CSLBCoP and Cont.-TrP, it consistently outperforms all other approaches with an encouraging margin in terms of both $\%ARP$ and $\%ARR$. Because total retrieval time is affected by feature dimensions, we find that NSST-LBNDP has a longer total retrieval time than LDEP, LWP, LBDP, LBDISP, LBPDAP, and LBPANDP descriptors, but its performance is far superior (Table 4.13).

The use of NSST subbands to capture multiscale, translational invariance, and directional information provides a highly effective representation of an input image. The technique effectively captures both fine and coarse information by using bit-plane slices. This powerful encoding technique for the bit-plane slices improves over all other existing descriptors and achieves the best handcrafted feature based results in the literature.

Table 4.13: Comparative performance evaluation of NSST-LBNDP and other approaches in terms of total retrieval time (in seconds)

Method	LDEP[200]	LWP[201]	LBDP[81]	LBDISP[82]	LBPDAP[83]	LBPANDP[84]	CSLBCOP[114]	Cont.-TrP[202]	NSST-LBNDP
NEMA-CT	0.10	0.24	0.26	0.28	0.21	0.18	0.78	1.61	0.44
TCIA-CT	0.46	1.21	1.01	1.27	1.07	0.56	3.50	8.49	2.19
YORK-MRI	0.37	0.63	0.62	0.53	0.45	0.35	1.26	3.11	0.99

In Fig. 4.18 the top 15 retrieved images for one query image from NEMA-CT dataset, for various descriptors is shown. When compared to other approaches, the NSST-LBNDP descriptor finds more relevant images accurately. This visual result validates the proposed descriptor's retrieval superiority over existing descriptors.

In Fig. 4.19, the feature vectors of all bit-plane-based descriptors: LBDP, LBPDAP, LBDISP, LBPANDP, and NSST-LBNDP, are compared using interclass and intraclass image categories. $I1$ and $I2$ are part of the same class, while $I2$ and $I3$ are from separate classes. Fig. 4.19 shows the p.d w.r.t zero mean of feature vector differences for pictures $I1$-$I2$ (intraclass) and $I2$-$I3$ (interclass) for different descriptors (Fig. 4.19(d-e)). High variance from the zero mean indicates low feature similarity, while high amplitude indicates better feature vector similarities. Fig. 4.19(d-e) reveals that NSST-LBNDP features are better at matching intraclass images and distinguishing interclass images.

4.3 Summary

In this chapter, we have introduced two NSST based image feature descriptors that use bit-plane decomposition to extract coarse to very fine image information in NSST domain. Because of the susceptibility of NSST coefficients to local

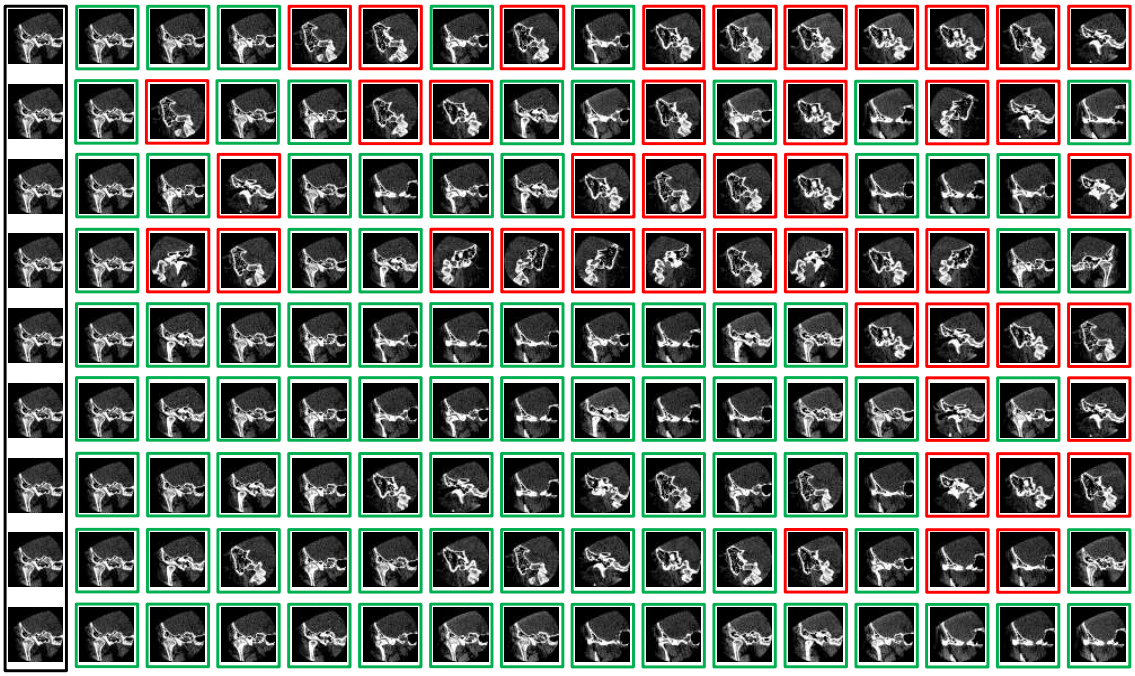

Figure. 4.18: Retrieved images obtained for the top 15 image matches in the NEMA-CT database for LDEP, LWP, LBDP, LBDISP, LBPDAP, LBPANDP, CSLBCoP, Cont.-TrP, and NSST-LBNDP descriptors. (The image inside the red box is incorrectly retrieved, the image inside the green box is correctly retrieved, and the image inside the black box is a query image.)

variations, the spatial domain bit-plane based descriptors cannot be implemented directly in NSST domain. An incorporation of non-linearity to NSST coefficients is important to distinguish the texture areas with like mean brightness and 2^{nd} order details. The first feature descriptor NSST-LBPDAP is an attempt to extend the existing spatial LBPDAP concept in NSST domain. In NSST-LBPDAP, addition of non-linearity and smoothing is performed on the NSST coefficients in each subband prior to bit-plane decomposition in order to limit the susceptibility of NSST coefficients to local variations. The bit-planes are encoded using existing LBPDAP encoding concept. We have demonstrated that the NSST-LBPDAP achieves encouraging improvement over the spatial LBPDAP version. However due to the inherent encoding nature of LBPDAP concept, the NSST-LBPDAP shows limitations in capturing many fine image details as LBPDAP considers only the 4 most significant bit-planes for encoding. Further the NSST-LBPDAP suffers from high dimensions.

Motivated from the success of NSST-LBPDAP, we introduce a new descriptor NSST-LBNDP which is based on bit-plane decomposition in NSST domain. This descriptor overcomes all the limitations of NSST-LBPDAP. After the incorporation of non-linearity, smoothing and normalization to NSST subband

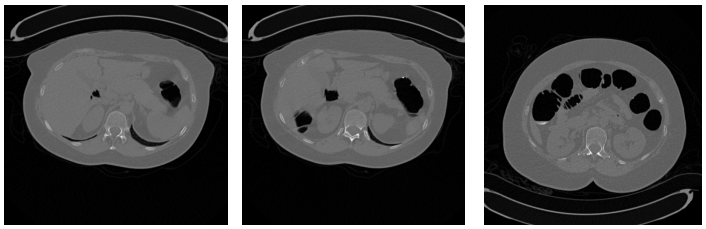

(a) I1 (b) I2 (c) I3

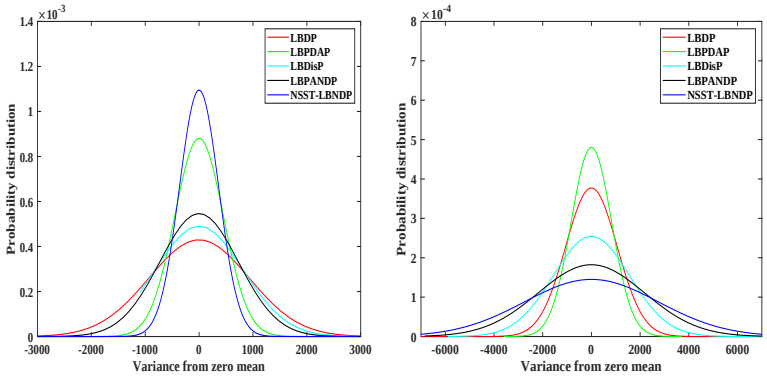

(d) Probability distribution(p.d) of feature vector difference(I1-I2) of intraclass images for different descriptors

(e) p.d of feature vector difference(I2-I3) of interclass images for different descriptors

Figure. 4.19: The illustration of distinguishing conduct of LBDP, LBPDAP, LBDISP, LBPANDP, and NSST-LBNDP features in discriminating interclass and intraclass images belonging to TCIA-CT

coefficients, the bit-plane decomposition is performed. After that, the encoded bit-plane are obtained by utilizing the effective relationship of dissimilarity between each neighboring bit and its adjacent neighbors. Finally, w.r.t each local reference the association between all the encoded bit-plane values and the corresponding reference local energy feature value is computed. This descriptor has low dimension than NSST-LBPDAP and Cont.-TrP.

Both these techniques are evaluated with experimental results obtained through experiments conducted in three publicly available biomedical image datasets. Both these approaches are observed to be effective compared to existing bit-plane based and local pattern based techniques. Performance evaluation in terms of %ARP and %ARR depicts the effectiveness of the proposed descriptors over the existing ones. The comparison of total retrieval time and feature dimension are also presented. From the experimental results it is observed that NSST-LBNDP performs superior to NSST-LBPDAP with less feature dimension.